Journal of The Electrochemical Society, **155** (9) K161-K165 (2008)
0013-4651/2008/155(9)/K161/5/$23.00 © The Electrochemical Society

Electrothermal Bonding of Carbon Nanotubes to Glass

Sriharsha V. Aradhya, Suresh V. Garimella, and Timothy S. Fisher[z]

School of Mechanical Engineering and Birck Nanotechnology Center, Purdue University, West Lafayette, Indiana 47907, USA

Applications that exploit the exceptional properties of carbon nanotubes (CNTs) at practical length scales almost invariably involve the fundamental issues of nanotube-to-surface contacts; indeed, interface properties often dominate mechanical, electrical, and thermal performance in devices and materials based on CNTs. In this paper we present a method to attach CNTs to glass surfaces and investigate the mechanism of bonding at the interface. An electric field which induces migration of alkali ions from glass into CNTs, with a reversed polarity as compared to an analogous anodic bonding configuration, is employed to form a chemical bond between nanotubes and glass. We report a pull-off force of 4.35 N/cm^2 averaged over the bonded area, with the possibility of localized areas of higher bonding strength.
 [DOI: 10.1149/1.2952814]

Manuscript submitted March 31, 2008; revised manuscript received June 5, 2008. Published July 22, 2008.

Carbon nanotubes (CNTs) have generated tremendous interest in recent years because of their excellent physical and chemical properties.[1] To exploit these properties at useful length scales, CNTs typically must interact with solid surfaces. To a large extent, these interfaces are dominated by van der Waals interactions,[2] which are often found to govern the mechanical behavior and transport characteristics of such structures. Being weak and of short range, van der Waals interactions can impede transport, and a need exists to replace this weak interaction with stronger, more reliable contacts.

While van der Waals interactions may provide significant mechanical adhesion over short ranges and increasing densities of filaments or nanotubes, transport properties as well as the ultimate achievable mechanical strength performance depend on bonding of individual nanotubes to surfaces. Ruoff and Lorents[3] discuss the importance of the binding interaction of CNTs to its surrounding materials and indicate that the creation of high-strength interfaces is a critical technological hurdle. They indicate that topological and chemical modification of CNTs may be critical in achieving high mechanical strength in single- and multiwalled CNT composites. The ability to synthesize vertically oriented CNT bundles enables structured contact topology, and hence, we are motivated to attempt chemical modification of the CNT interfaces to achieve high interfacial binding as the next step.

For improving mechanical contact between vertically aligned CNT arrays and metals, Zhao et al.[2] used prestressing loads on the order of 400 N/cm^2 and obtained a pull-off force on the order of 10 N/cm^2 for contacts intended for use as dry adhesives. They reported a strong dependence on the bonded area, with the pull-off force decreasing from 10 N/cm^2 for 4 mm^2 samples to 2 N/cm^2 for samples with 10 mm^2 nominal area. They also indicated the bonding force to be significant compared to the best-known natural material, the feet of Gecko (10 N/cm^2), and other synthetic bio-inspired dry adhesive materials (0.003–3 N/cm^2).

Thermal transport across CNTs in suspension has been shown to be substantially limited because of interfacial resistance by Huxtable et al.,[4] and a related molecular dynamics simulation study[5] also indicated that this low resistance is due to the absence of covalent bonding that would couple to the higher energy phonon states. Theoretical modeling by Prasher[6] has shown that thermal interface resistances of nanosized constrictions are higher than values predicted by continuum transport considerations. Son et al.[7] conducted photothermoelectric measurements on CNT–Si/SiO_2 growth interfaces and found the interfacial resistance to be significantly higher than the predictions of Prasher.[6] They explained this discrepancy as arising from mechanical imperfections and the presence of growth catalyst in the experiments that were not accounted for in the idealized model. Cola et al.[8] studied thermal contact resistance between vertically oriented CNT arrays contacting silver surfaces experimentally and demonstrated that the free nanotube tip resistance dominated the overall resistance within the stack of resistances between the growth substrate and the contacting metal (Fig. 1a).

With regard to electrical transport, there is tremendous interest in using CNTs as quasiballistic transport channels for transistor[9] and interconnect[10] applications. Contact resistance has been shown to be important in these applications as well,[11] and reducing the tunneling barrier at van der Waals-dominated nanotube contacts has been attempted with pulsed annealing[12] and electroless metal deposition.[13]

In the present study, we seek to increase the area of contact as well as the quality of contact between CNTs and the contacting surface. We present a straightforward method of bonding CNTs to glass surfaces and elucidate the salient mechanism of this bonding, which appears to involve bonding of carbon and oxygen at the CNT–glass interface. Specifically, we focus on electrothermal bonding as a practical technique that would require low-to-moderate temperatures and voltage biases because of the field enhancement and possible ion absorption effects enabled uniquely by the CNTs.[14] We focus on the chemical modifications and interfacial mechanical enhancement in this study as the first steps in understanding the enhancement of interfacial thermal transport that we have achieved.[15]

Experimental

Figure 1b shows a scanning electron microscopy (SEM) image of a typical vertically oriented CNT array grown by microwave plasma chemical vapor deposition (MPCVD) using a trilayer catalyst[16] of 30 nm Ti, 10 nm Al, and 3 nm Fe on a silicon wafer. After annealing the Si wafer in a nitrogen atmosphere in the MPCVD reactor, CNTs were grown under the following processing conditions: 900°C with 50 sccm H_2, 10 sccm CH_4, and at 300 W microwave plasma power and 10 Torr pressure. The length of CNTs depends on the duration of the process. We have grown and bonded CNTs with lengths in the range of 30–100 μm.

Anodic bonding is a standard procedure in microfabrication.[17] This process bonds silicon wafers to glass by creating an oxide layer at the interface between silicon and glass[18,19] and is enabled by the movement of alkali ions, Na^+ or K^+, depending on the type of glass used. The name of the process derives from the fact that the alkali ions are driven from Si anode region toward the cathode, which is in contact with the glass side. This ion flow and consequent transfer of charge creates a charge inversion layer at the Si–glass interface. The oppositely charged surfaces are attracted, creating intimate contact, and oxidation at the interface leads to a strong bond. A weakening of this bond has also been demonstrated to occur due to the reversal of current.[20] In the present work, we use this migration of alkali ions in a modified protocol to exploit alkali intercalation characteristics of CNTs.

Figure 2 illustrates the setup used for bonding CNT arrays grown on a silicon substrate to bulk glass. A glass slide (Corning Pyrex 7740, thickness 650 μm, and area approximately 5 × 5 mm) is connected to the positive terminal, and the Si wafer is connected to

[z] E-mail: tsfisher@purdue.edu

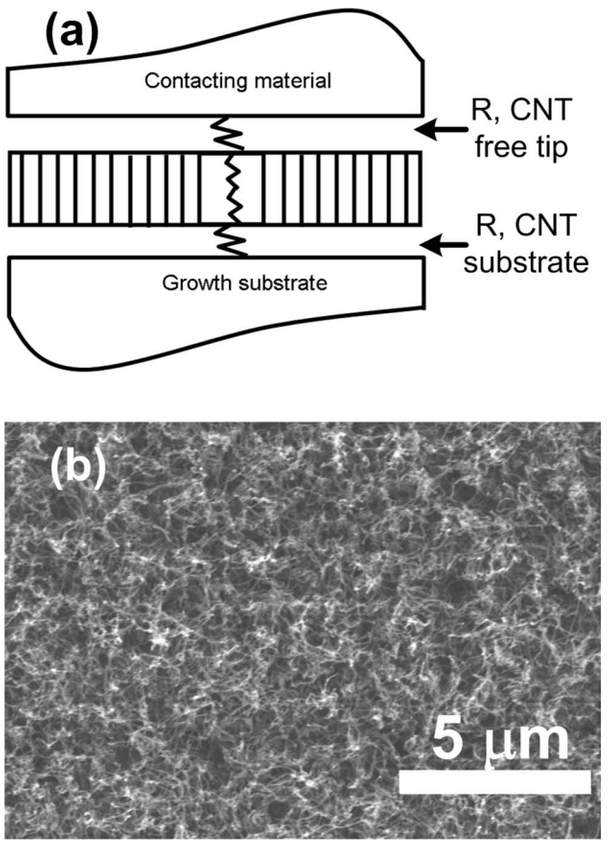

Figure 1. (a) Schematic illustration of a CNT-based thermal interface material showing relevant thermal resistances. (b) SEM image of as-grown, vertically aligned CNT arrays (top view).

the negative terminal of the power supply. We have qualitatively observed good postbonding adhesion of the CNTs to the glass surface for applied voltages above 800 V and bonding process temperatures above 200°C. The bonding process persists for 30 min, after which the glass surface adheres well to the CNT array. This bonding is quantified in this work in terms of the force required to separate the CNT array from glass. Because of the reversal of polarity as compared to conventional anodic bonding, charges move in the opposite direction, as shown in Fig. 2. We interpret the mechanisms for bonding of CNTs to glass through the measured variation of current

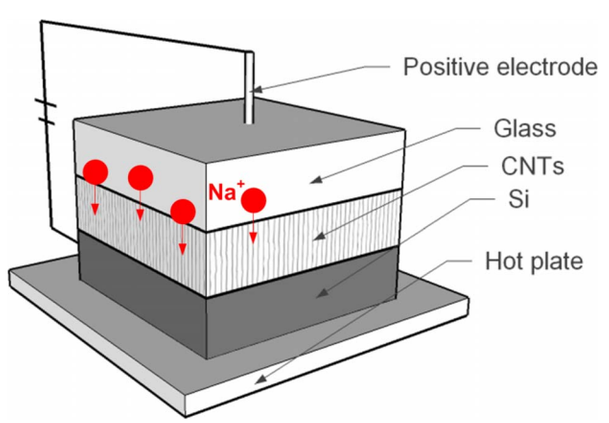

Figure 2. (Color online) Schematic illustration of the CNT bonding setup indicating the migration of alkali ions.

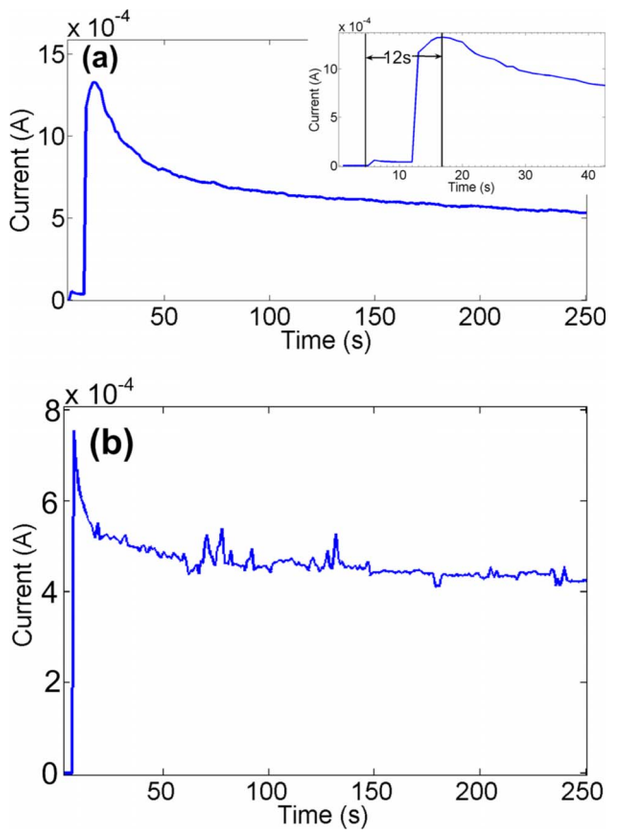

Figure 3. (Color online) Bonding current as a function of time for typical CNT–glass bonding experiments: (a) bonding using a 650 μm glass slide at 400°C with 1000 V (inset: expanded view of the delay between turn-on and the peak current), and (b) bonding with 2.5 μm thin film of glass on a silicon wafer at 175°C and 100 V.

with time over the bonding period, SEM images of the bonded interface, and X-ray photoelectron spectroscopy (XPS) spectra.

Results and Discussion

The usage of glass layers is motivated by two reasons. From transport considerations, the usage of thin layers of evaporated glass (2.5 μm in this study) is expected to contribute relatively low thermal resistances of about 2.5 mm^2 K/W. We believe that by optimization of glass thickness and bonding parameters, it may be possible to achieve enhanced conduction at the interface compared to bare CNTs. Also, we seek to understand the mechanism of bonding with the known chemistry of glass in order to replace glass with higher conductivity materials or processed surfaces with suitable chemistries.

Bonding current is a useful macroscopic quantity to monitor the process. Figure 3a shows the variation of current with time for a bonding process with a voltage of 1000 V imposed across the Si–glass–CNT–Si stack held at 400°C. A clear peak exists in the current and corresponds to the migration of alkali ions from the glass toward the CNTs. The time taken for the current to reach a peak is a measure of the drift speed of the alkali ions through the glass, and this speed is expected to depend on the magnitude of electric field inside the glass, as we have confirmed with a different experiment in which CNT arrays are bonded to thin films of glass.

For this second set of experiments, we bonded CNTs to thin films of evaporated glass of 2.5 μm thickness on a silicon wafer. In this case, bonding occurs at lower temperatures and voltages than for the thicker glass slide considered above. This result is expected because of the smaller total distance in this case for diffusion of the alkali

ions and the higher electric field within the glass thin film. Figure 3b shows the bonding current profile for the Si–glass–CNT–Si stack at a voltage of 100 V and at a temperature of 175°C. These conditions are chosen so that the currents for the thin-film glass bonding are comparable to those measured while bonding the thicker glass slide (Fig. 3a). The current again shows a peak, but the time required to reach the peak is smaller, for the reasons already discussed which allow for bonding at lower temperature and voltage. Also, greater signal noise is observed in this case and may be attributed to the increased relative roughness of the evaporated glass caused by the processing conditions during deposition.

SEM images of a cross section of the contact surfaces after bonding reveal good adhesion between the glass thin film and the CNT array (Fig. 4a). At some locations on the sample, we observe that some CNTs are separated from the growth substrate but remain adhered to the glass surface (Fig. 4b).

We have estimated the bond strength from the force needed to separate the CNT array from the 650 μm thick glass surface. For this measurement (Fig. 5), the CNT side of the test specimen, bonded for 30 min at 200°C, is attached to a laboratory weighing scale. The glass side is then attached to a cantilever and the CNT array is separated from the glass slide surface manually. Horizontal orientation of the cantilever and all concerned surfaces and careful pull-off of the bonded interface enables a good estimate of the normal adhesive force at the interface, and this force is measured to be 1.2 N. We note that some solid residue remained on the glass slide surface (Fig. 6a) and was confirmed to be CNTs by SEM imaging (Fig. 6b). Unbonded CNT arrays (heated to the same temperature for 30 min but not subject to electrostatic bonding) separated at a load of less than the measurable resolution of 0.001 N.

It is difficult to accurately quantify the area over which bonding occurs in order to calculate the strength per unit area. We observe that the area with CNT residue on the glass is 5.34 × 5.17 mm,

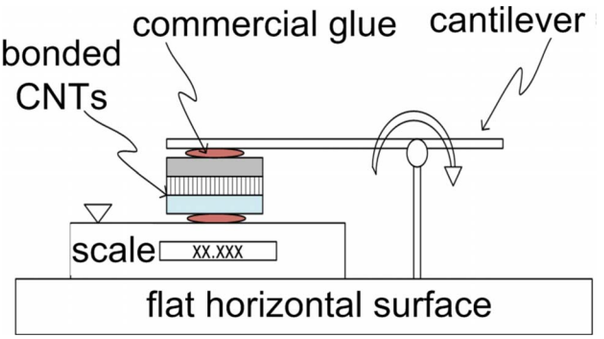

Figure 5. (Color online) Experimental apparatus for estimation of interfacial bonding strength.

which is roughly the entire area of the CNT array specimen used for bonding. Using this value of area for normalizing the force, we calculate an apparent bond strength of 4.35 N/cm^2. Another similarly sized sample bonded under identical conditions was measured to have a pull-off force of 1.4 N, demonstrating the consistency of the process. The significance of our bonding force can be understood by comparing it to values reported by Zhao et al.[2] Their study used samples that were smaller in area, contained shorter CNTs, and were mechanically loaded with an applied pressure that was 2 orders of magnitude higher than the force on our samples during bonding. All three of these factors were identified as being responsible for producing higher adhesive forces in their study. They also characterized

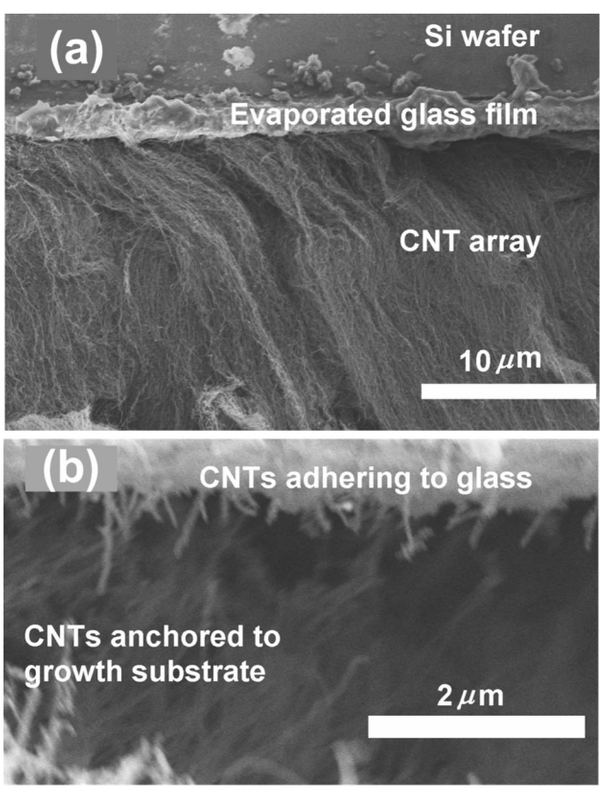

Figure 4. (a) CNT array adhering to a thin film of glass, and (b) CNTs locally stripped from substrate while still adhering to the glass surface. The glass layer of 2.5 μm thickness may be seen in the top part of both images.

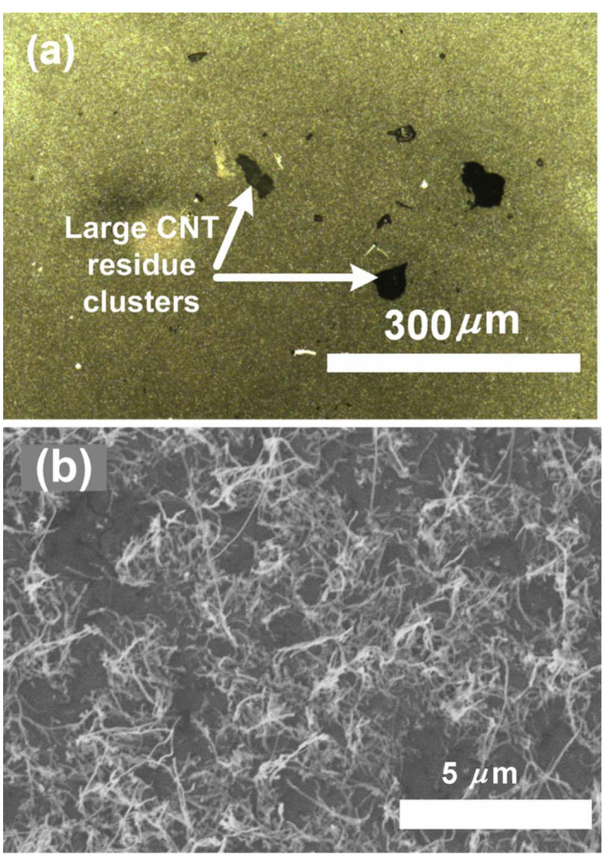

Figure 6. (Color online) (a) Optical microscope image of glass surface at 5× magnification, and (b) SEM image showing residual CNTs on the surface of 650 μm glass slide after separation of the bonded CNT array.

Table I. Elemental distribution in glass before and after bonding by XPS with key species highlighted.

Peak	Before bonding (Atomic %)	After bonding (Atomic %)
B 1s	2.25	1.57
C 1s	10.90	25.95
Ca 2p	0.44	0.20
Cl 2p	0.00	0.70
F 1s	0.00	0.77
N 1s	0.49	0.00
Na 1s	2.49	12.54
O 1s	57.67	43.46
Si 2p	25.52	14.67
Zn 2p	0.23	0.15

their adhesive force as arising from van der Waals interactions. The comparable adhesive forces in our study are thus a result of chemical forces beyond the van der Waals force, as the applied pressure during bonding in our experiment is negligible compared to the large prestress used to achieve van der Waals adhesion. This conclusion is strengthened by a detailed study of chemical modification at the interface.

To further study the mechanism of bonding, XPS spectra were obtained using a Kratos Ultra DLD spectrometer with monochromatic Al $K\alpha$ radiation ($h\nu$ = 1486.69 eV) to analyze the chemical composition before and after bonding. First, the 650 μm glass slide and CNT array surfaces were analyzed before bonding. After the bonding process was completed, the glass-slide-bonded surface was separated from the CNT-array-bonded surface and analyzed separately with XPS (the surfaces are referred to as "glass surface" and "CNT surface," respectively, in the following).

Table I lists the chemical concentrations obtained through XPS spectra for the glass samples before and after bonding. The sodium peak increases fivefold after the bonding process. Migration of sodium toward the CNT surface confirms the expected direction of migration of the alkali ions for the applied polarity. The increase in carbon percentage can be identified with the CNT residue on the glass surface after bonding, as evidenced previously from Fig. 6.

In Table II, the chemical changes on the CNT surface before and after bonding are quantified. The additional sodium content after bonding is clearly apparent. The high-resolution C 1s XPS spectrum for the CNT surface before bonding is shown in Fig. 7. The C 1s peak in graphitic carbon is known to be asymmetric and is fitted using a hybrid Doniac–Sunjic/Gaussian–Lorentzian line shape.[21] This line shape captures the asymmetry of the graphitic peak and helps to establish the asymmetry parameter,[22] which is useful in assessing changes to carbon that is bonded to a glass surface. We observe no major change in the high-resolution C 1s spectrum of the CNT array surface after bonding, indicating that most of the CNTs which remain anchored to the growth substrate do not undergo a chemical change.

Figure 8a contains a high-resolution XPS spectrum of the glass surface around the C 1s peak before bonding. The fitted curves correspond to different oxidized states of carbon that are similar to contaminants identified on glass surfaces from a study by Ochs et

Table II. Elemental distribution on CNT array surface before and after bonding obtained by XPS analysis.

Peak	Before bonding (Atomic %)	After bonding (Atomic %)
C 1s	99.29	91.88
Na 1s	0.00	2.93
O 1s	0.71	4.74
Cl 1p	0.00	0.21
F 1s	0.00	0.24

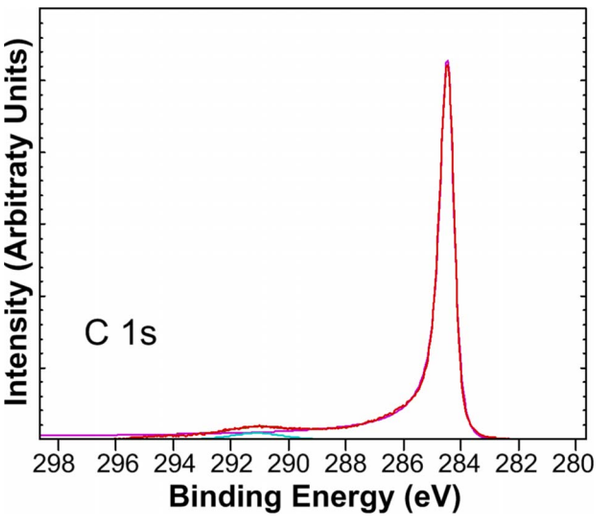

Figure 7. (Color online) High-resolution scan C 1s of CNT array surface before bonding. Red plot represents raw data.

al.[23] through an XPS study. The study also indicated that these carbon contaminants reduce with the heating of the glass surfaces. This reduction in the contaminant species is also observed here in the spectrum of the C 1s region after the bonding process in Fig. 8b. The spectrum is significantly different, with a sharp C 1s peak corresponding to a CNT graphitic peak at a binding energy of 284.5 eV, as opposed to the broader, aliphatic carbon peaks in Fig. 8a. The

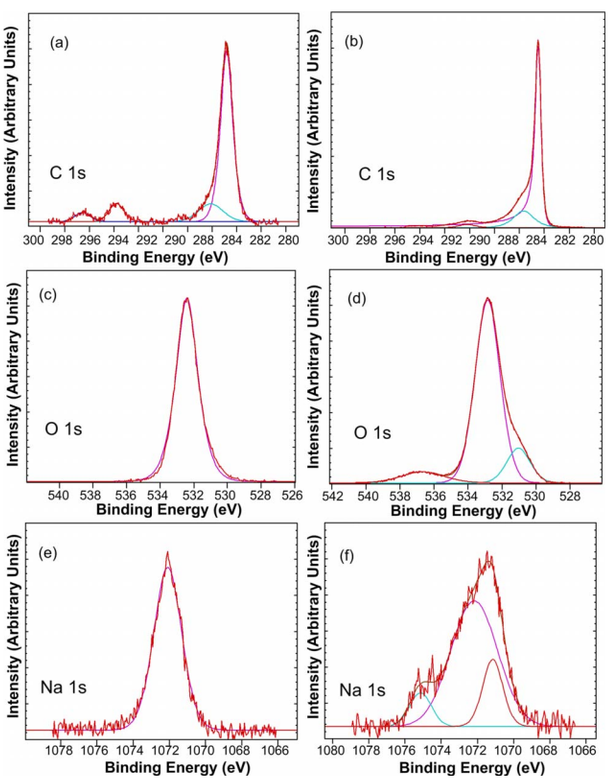

Figure 8. (Color online) Fitted XPS spectra. Before bonding: (a) C 1s on glass, (c) O 1s on glass, and (e) Na 1s on glass. After bonding: (b) C 1s on glass, (d) O 1s on glass, and (f) Na 1s within CNT array. Red plot represents raw data.

total carbon content on the glass surface also increases after bonding and separation, as noted in Table I. This result suggests that the carbon spectrum in Fig. 8b is primarily caused by the graphitic carbon of the CNTs adhering to the glass surface. A broad peak at about 290 eV attributed to π–π^* transitions also appears, indicating the presence of CNTs on the glass surface.[24] For these reasons, we use the same asymmetric profile that fits the CNT surface spectrum (Fig. 7) to analyze the C 1s spectrum on the glass surface after bonding in Fig. 8b. Significantly, the shoulder of the sharp graphitic peak can be decomposed into a symmetric peak at about 286 eV, corresponding to an oxidized state of carbon present on the glass surface.

The high-resolution oxygen (O 1s) spectrum of the glass surface before bonding in Fig. 8c is fitted with a symmetric peak at 532.4 eV. After bonding, the O 1s spectrum in Fig. 8d shows evidence of three different states of oxygen, two of which differ by more than 1 eV from the initial oxygen peak in Fig. 8c. These two peaks can be assigned to C═O (531.03 eV) and H–O (536.7 eV) and are consistent with a study on CNT sensitivity to oxidation by Martinez et al.[25] Oxidation of carbon indicated by Fig. 8b and the appearance of two new oxygen states in Fig. 8d together illustrate a significant result that oxygen atoms bond the carbon atoms in CNTs to the glass surface.

XPS scans of sodium on the glass surface reveal in detail the central role of alkali migration in this bonding process. Figure 8e shows the sodium peak on the glass surface before bonding. This spectrum can be fitted with a single peak, which corresponds to the typical Na_2O binding energy value of the sodium as expected in Pyrex glass.[26] The sodium spectrum on the CNT surface after bonding shown in Fig. 8f illustrates the emergence of two additional species of sodium. The low-binding-energy (1071.15 eV) peak can be assigned to Na_2CO_3, $NaHCO_3$, NaF, and presumably NaCl, which are the possible migrated species as indicated in Table II. The high-binding-energy (1075.15 eV) peak, however, is more interesting because it is near the elemental value of sodium, 1078 eV. This observation suggests that these species of sodium are the intermediately oxidized (between 0 and +1) states of sodium present within the CNTs.[27] This explanation is consistent with an alkali intercalation study by Cupolillo et al.[28] and provides a complementary validation by XPS analysis.

Conclusion

We have developed a new method of bonding CNTs to a glass surface and have shown that the mechanism of this bonding appears to involve migration of alkali ions into CNTs. Bonding pull-off forces of approximately 4 N/cm^2 were measured and are significant when compared to pure van der Waals interaction forces. Optimizing the length of the CNTs and the preloading during bonding has the potential to increase this bonding force. This bonding is also expected to improve interfacial thermal transport because of a direct pathway created by bonding of the CNT tips to the contacting surface. The elastic nature of CNTs is expected to provide a robust mechanical interface by accommodating the mismatch in the coefficient of thermal expansion between contacting surfaces. The alkali drift mechanism suggests many applications that involve the bonding of CNTs to surfaces that are naturally or artificially impregnated with suitable mobile ions.

Acknowledgments

The authors acknowledge stimulating discussions with, and experimental support from, Baratunde Cola and Ben Jones. We thank Dmitry Zemelyanov for XPS data and the National Science Foundation Cooling Technologies Research Center for funding this project.

Purdue University assisted in meeting the publication costs of this article.

References

1. M. S. Dresselhaus, G. Dresselhaus, and A. Jorio, *Annu. Rev. Mater. Res.*, **34**, 247 (2004).
2. Y. Zhao, T. Tong, L. Delzeit, A. Kashani, M. Meyyappan, and A. Majumdar, *J. Vac. Sci. Technol. B*, **24**, 331 (2006).
3. R. S. Ruoff and D. C. Lorents, *Carbon*, **33**, 925 (1995).
4. S. T. Huxtable, D. G. Cahill, S. Shenogin, L. Xue, R. Ozisik, P. Barone, M. Usrey, M. S. Strano, G. Siddons, M. Shim, et al., *Nat. Mater.*, **2**, 731 (2003).
5. S. Shenogin, L. Xue, R. Ozisik, P. Keblinski, and D. G. Cahill, *J. Appl. Phys.*, **95**, 8136 (2004).
6. R. Prasher, *Nano Lett.*, **5**, 2155 (2005).
7. Y. Son, S. K. Pal, T. Borca-Tasciuc, P. M. Ajayan, and R. W. Siegel, *J. Appl. Phys.*, **103**, 024911 (2008).
8. B. Cola, J. Xu, C. Cheng, X. Xu, T. S. Fisher, and H. Hu, *J. Appl. Phys.*, **101**, 054313 (2007).
9. A. Javey, J. Guo, Q. Wang, M. Lundstrom, and H. Dai, *Nature (London)*, **424**, 654 (2003).
10. M. Nihei, M. Horibe, A. Kawabata, and Y. Awano, *Proc. IEEE Interconnect Technology Conference*, IEEE, p. 251 (2004).
11. J. Tersoff, *Appl. Phys. Lett.*, **74**, 2122 (1999).
12. Y. Woo, G. S. Duesberg, and S. Roth, *Nanotechnology*, **18**, 095203 (2007).
13. R. Seidel, M. Liebau, G. S. Duesberg, F. Kreupl, E. Unger, A. P. Graham, and W. Hoenlein, *Nano Lett.*, **3**, 965 (2003).
14. X. Z. Wang, M. G. Li, Y. W. Chen, R. M. Cheng, S. M. Huang, L. K. Pan, and Z. Sun, *Electrochem. Solid-State Lett.*, **9**, E23 (2006).
15. S. V. Aradhya, S. V. Garimella, and T. S. Fisher, in *Proceedings of the Eleventh Intersociety Conference on Thermal and Thermomechanical Phenomena in Electronic Systems*, IEEE and ASME, p. 1071 (2008).
16. J. Xu and T. S. Fisher, *IEEE Trans. Compon. Packag. Tech.*, **29**, 261 (2006).
17. W. H. Ko, J. T. Suminto, and G. J. Yeh, in *Micromachining and Micropackaging of Transducers*, C. D. Fung, P. W. Chung, W. H. Ko, and D. G. Fleming, Editors, p. 41, Elsevier Science, New York (1985).
18. P. Yu, Ch. Pan, and J. Xue, *Mater. Lett.*, **59**, 2492 (2005).
19. P. Nitzsche, K. Lange, B. Schmidt, S. Grigull, U. Kreissig, B. Thomas, and K. Herzog, *J. Electrochem. Soc.*, **145**, 1755 (1998).
20. J. A. Plaza, E. Gonzalez, J. Esteve, M. M. Visser, D. T. Wang, and A. Hanneborg, *Electrochem. Solid-State Lett.*, **3**, 392 (2000).
21. CasaXPS software reference manual (2006).
22. J. Diaz, G. Paolicelli, S. Ferrer, and F. Comin, *Phys. Rev. B*, **54**, 8064 (1996).
23. D. Ochs, S. Dieckhoff, and B. Cord, *Surf. Interface Anal.*, **30**, 12 (2000).
24. H. Estrade-Szwarckopf, *Carbon*, **42**, 1713 (2004).
25. M. T. Martinez, M. A. Callejas, A. M. Benito, M. Cochet, T. Seeger, A. Anson, J. Schreiber, C. Gordon, C. Marhic, O. Chauvet, et al., *Carbon*, **41**, 2247 (2003).
26. P.-Y. Brisson, H. Darmstadt, M. Fafard, A. Adnot, G. Servant, and G. Soucy, *Carbon*, **44**, 1438 (2006).
27. J. P. Lukaszewicz, *J. Math. Sci.*, **32**, 6063 (1997).
28. A. Cupolillo, C. Giallombardo, and L. Papagno, *Surf. Sci.*, **601**, 2828 (2007).